Available online at www.sciencedirect.com

ScienceDirect

Proceedings of the Combustion Institute 37 (2019) 1023–1030

Proceedings of the Combustion Institute

www.elsevier.com/locate/proci

Trace metal assisted polycyclic aromatic hydrocarbons fragmentation, growth and soot nucleation

Qian Mao [a], Kai H. Luo [a,b,*]

[a] *Department of Energy and Power Engineering, Center for Combustion Energy, Key Laboratory for Thermal Science and Power Engineering of Ministry of Education, Tsinghua University, Beijing 100084, China*

[b] *Department of Mechanical Engineering, University College London, Torrington Place, London WC1E 7JE, UK*

Received 30 November 2017; accepted 13 June 2018

Available online 6 July 2018

Abstract

The present work demonstrates the role of trace metal, namely Fe, on the polycyclic aromatic hydrocarbons (PAHs) fragmentation, growth and soot nucleation through performing reactive molecular dynamics (MD) simulations with the ReaxFF force field. The structure of the Fe–PAH complex and the diffusivity of the Fe atoms on the PAH surface are scrutinized at different temperatures. A series of binary collisions between a Fe atom and a PAH molecule are systemically investigated to clarify the influence of Fe collision energy, collision orientation and equilibrium temperature of the PAH molecule on the PAH fragmentation. The simulation results indicate that Fe collision on PAH molecules at a typical flame temperature, i.e., 1500 K, is sufficient to break the C–H and/or C–C bonds by forming PAH radicals with Fe bonded. In contrast to the largest PAH clusters composed of PAH dimers or trimers in pure PAH systems at flame temperatures, presence of Fe atoms dramatically enhances the PAH growth and soot nucleation rate as the Fe atoms significantly lower the PAH fragmentation temperature. Moreover, the soot nucleation pathway is found to be dependent on temperature. At 1500 K, Fe atoms preferentially break the C–H bonds and connect the PAHs through dehydrogenation. Eventually, Fe atoms merge with the aromatic rings and facilitate the formation of embedded five/seven-membered rings during PAH growth at elevated temperatures. Results from this study contribute to further understanding of the dynamic physicochemical processes in soot formation during more realistic combustion with trace metals.

Keywords: Fe; Polycyclic Aromatic Hydrocarbon (PAH); Soot; Molecular dynamics (MD)

1. Introduction

Polycyclic aromatic hydrocarbons (PAHs) and the subsequent formation of soot particles have drawn substantial research and public interest

* Corresponding author at: Department of Mechanical Engineering, University College London, Torrington Place, London.

E-mail address: k.luo@ucl.ac.uk (K.H. Luo).

https://doi.org/10.1016/j.proci.2018.06.106

as soot is a notorious environmental and health hazard [1–10]. Nucleation is a critical step in soot formation, which starts from gas phase PAH monomers and yields condensed nascent soot particles. There is, however, still a lack of fundamental understanding of the mechanisms for above process. The widely reported soot nucleation pathway, which involves the dimerization of PAHs into stacks, is debatable according to previous experimental and theoretical studies [2,8,10–13]. It is accepted that some stronger interactions are prerequisite for soot nucleation at flame temperatures [2].

Trace metals, such as Na, K, Al, and Fe, are present in practical hydrocarbon fuels and engine lubricating oils at PPM levels [14–22]. According to the quantum chemistry calculations, cation (Na^+, Mg^{2+}, Fe^{2+}) increases the binding energy of PAHs, and it is strong enough to stabilize the dimers at flame temperatures [22]. However, studies by Feitelberg et al. [16] reported that the iron compounds of ferrocene dissociate well as free Fe atoms in gas phase (above 1750 K) before soot inception. The volatile organometallic compound of ferrocene is one of the most common Fe additives in engines, which is found to have soot enhancing as well as suppressing characteristics in flames [14–21]. That is, the dissociated Fe atoms participate in the PAH growth and soot inception as observed by the increased soot particle size and volume fraction in primary flame zones. Subsequently, in the soot oxidation or burnout stage, Fe is oxidized and its oxides facilitate soot oxidation as oxidative catalysts thereby reducing soot emission [14–21].

Majority of the previous studies on Fe contribution to soot formation were restricted to experiments, and most of them focused on its role on the soot reduction [14–21]. Moreover, the resulting structures of soot particles formed with iron additives were not characterized in detail, and fundamental understanding of the soot enhancing characteristics from the molecular growth and soot inception by Fe additives has not been assessed yet. Furthermore, the interplay between Fe atoms and PAHs at the atomic level are still unclear. In addition, there is much ambiguity regarding the dynamic processes involving the PAH fragmentation, molecular growth and soot inception in the presence of Fe atoms.

The present study attempts to provide a fresh insight into the role of Fe atoms on the PAH fragmentation, PAH growth and soot inception via molecular dynamics (MD) simulations with the ReaxFF force field. We examine the diffusivity of Fe atoms on the PAH surface, PAH structures generated from Fe collisions, PAH growth pathways and soot nucleation mechanisms in the presence of Fe atoms. To qualify and quantify the role of metallic Fe atoms, we present a comparison of the results with our previous work [11] on soot nucleation in pure PAH systems.

2. Methodology

2.1. Simulation details

In this study, the impact of Fe atoms on PAH fragmentation, PAH growth and soot nucleation is investigated at varied temperatures. Coronene is selected as a representative PAH. Typically, the ferrocene precursor is added to flames at PPM level [14–21] and dissociates well above 1750 K by forming metallic iron atoms before soot inception [16]. The ionization energies from Fe to Fe^{1+} and Fe^{2+} are 759.3 and 2320.3 kJ/mol, respectively [23]. Based on Saha equilibrium [24], the number densities of Fe^{1+} and Fe^{2+} are found to be about 10^{-3} and 10^{-24} cm^{-3} at 1500 K as the number density of electron is about $10^{10\text{-}11}$ cm^{-3} in flames [25]. Thus, the metallic Fe is chosen to represent the trace metal in this study.

To study the diffusivity and binding of the Fe atom on PAHs, the Fe-coronene complex is firstly built with the Fe atom locating at the center of the coronene surface. Before conducting the MD simulation, energy minimization of the coronene molecule and Fe–coronene complex is performed by the conjugate gradient (CG) algorithm. Thermal equilibrium of the optimized Fe–PAH complex is studied in the canonical ensemble (NVT) and the temperature is maintained constant by the Nosé–Hoover thermostat of 500 K, 1000 K and 1500 K. To study the effects of Fe atoms on PAH fragmentation, a series of binary collisions between a Fe atom and a coronene molecule at varied collision energies and orientations are performed adiabatically using the microcanonical ensemble (NVE) with a time step of 0.1 fs to ensure the conservation of energy during the high-energy collision. Finally, ReaxFF-MD simulations of PAH growth and soot inception with and without the presence of Fe atoms are performed in a cubic box with periodical boundary conditions in the NVT ensemble at temperatures from 1500 to 2500 K. The initial number density of PAH molecule is selected to be 2×10^{18} cm^{-3}, which is the same as those reported by Violi et al. [10] and Kraft et al. [13]. That is, if the PAH monomer is about 1×10^{15} cm^{-3} in flames, 1 ns of MD simulation time at current initial setup corresponds to 8.5 ms in laboratory combustion [10]. In this study, MD simulations are performed using Large-scale Atomic/Molecular Massively Parallel Simulator (LAMMPS) package [26]. Snapshots and movies in this study are prepared by Visual Molecular Dynamics (VMD) [27] and Open Visualization Tool (Ovito) [28].

2.2. Simulation method

Complex interactions between Fe atoms and PAH molecules are described with a general bond-order-based potential, namely the ReaxFF force field [29,30]. Molecular dynamics simulation

with the ReaxFF force field can simulate reactive systems that are not amenable to classical MD methods. In the meantime, it is capable of handling substantially larger reactive systems over a much longer timescale than quantum mechanism [30]. The ReaxFF force field with C/H/Fe description employed in this study was obtained through extensively training against data from quantum chemistry calculations by considering the atom, bond, off-diagonal bond, angle parameters for interactions among Fe, C and H [29,31,32]. Specifically, parameters between Fe and C/H are derived from a series of density functional theory (DFT) calculations of the iron surface formation energies, binding energies of hydrocarbon radicals on different iron surfaces and the barrier heights of surface reactions based on generalized gradient approximation (GGA) with the Perdew–Burke–Ernzerhof (PBE) method for exchange-correlation functional [32,33]. Parameters between C and H are derived through training against DFT calculations based on the B3LYP/6-311G** method [29,34,35]. The van der Waals interaction for carbon is additionally described by PBE exchange–correlation functional with the DFT-D2 parameters [31,36]. Detailed parameter sets for C/H/Fe are attached to the Supplemental Material as Table S1.

To the best of our knowledge, studies of metallic Fe–PAH systems are few and far between, which are only limited and restricted to systems of benzene absorption on Fe surfaces [37] and Fe atoms in graphene vacancies [38]. Validation of the ReaxFF force field is mostly done through comparison with DFT calculations. For example, the binding energy of benzene located on Fe (100) surface at the hollow site calculated by the ReaxFF force field (27.16 kcal/mol) is comparable to that from the DFT calculation (24.67 kcal/mol) [37]. In addition, the C/H description in this ReaxFF force field has been proved to accurately predict the boiling/sublimation temperatures of PAHs [11]. Thus, the ReaxFF force field is currently the best choice for describing metallic Fe-PAH system of such complexity in terms of computational expense and accuracy.

3. Results and discussion

Temperature dependent structure of the Fe–PAH complex is scrutinized in Section 3.1. Section 3.2 discusses the Fe collision energy, orientation and PAH temperature on the PAH fragmentation and resulting structures. Section 3.3 focuses on revealing the PAH growth pathway and soot nucleation mechanism with and without the presence of Fe atoms.

3.1. Fe–PAH complex

Structure of the Fe–PAH complex is a key factor that significantly affects the subsequent PAH growth and soot nucleation. Since temperature is critical to determine the diffusivity, diffusion of Fe atoms on the surface of coronene molecule is investigated at different temperatures. A parameter, namely normalized displacement (δ), is proposed to quantitatively evaluate the diffusivity of the Fe atom on the coronene surface and expressed as,

$$\delta = \sqrt{\mathrm{MSD}}/d_{\mathrm{aromatic}} \tag{1}$$

where d_{aromatic} is the diameter of a six-membered aromatic ring, MSD is the mean squared displacement that is a measurement of diffusivity,

$$MSD = (x_{\mathrm{Fe}_t} - x_{\mathrm{Fe}_0})^2 + (y_{\mathrm{Fe}_t} - y_{\mathrm{Fe}_0})^2 + (z_{\mathrm{Fe}_t} - z_{\mathrm{Fe}_0})^2 \tag{2}$$

where x_{Fe_0}, y_{Fe_0}, and z_{Fe_0} are the position of the Fe atom after optimization, x_{Fe_t}, y_{Fe_t}, z_{Fe_t} are the position of the Fe atom in determined time t [39]. Changes in the normalized displacement (δ) of the Fe atom on the coronene surface at 500, 1000 and 1500 K are displayed in Fig. 1. Apparently, the normalized displacement remains almost constant during the equilibrium process at 500 and 1000 K. Meanwhile, the trajectory of the Fe atom from 0 to 400 ps is recorded as shown in the blue line in insert (b) of Fig. 1, which illustrates that the Fe atom almost locates at the center of the coronene surface at 1000 K. Nevertheless, the dynamic behavior of the Fe atom is entirely different at 1500 K. The increase of the normalized displacement at about 30 ps results from the hopping of the Fe atom to the outer aromatic ring (1) as indicated by the insert (c) in

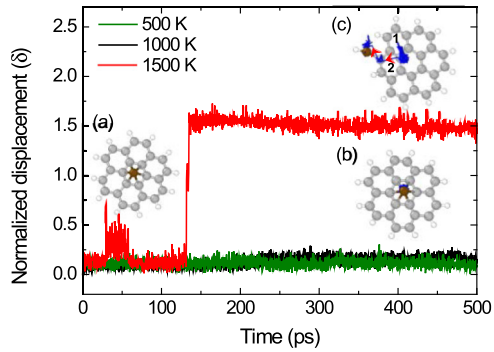

Fig. 1. Normalized displacement of a Fe atom on the coronene surface at 500 K, 1000 K and 1500 K. The inserted snapshots are structures of Fe–coronene complexes at different temperatures: (a) initial optimized structure after energy minimization, (b) structure at 400 ps, 1000 K with the blue line representing the trajectory of the Fe atom from 0 to 400 ps, (c) structure at 400 ps, 1500 K with the blue line representing the trajectory of the Fe atom from 0 to 400 ps and red arrows indicating the hopping directions (C atom: grey, H atom: white, Fe atom: ochre). (For interpretation of the references to color in this figure legend, the reader is referred to the web version of this article).

Fig. 1. This structure, however, is not thermodynamically stable and the Fe atom hops back to the center of the coronene after 60 ps as the normalized displacement decreases. Theoretical modeling studies of Fe atoms on a graphene surface predict that a migration barrier is smaller than 1 eV, and it should be even smaller on PAH surface with limited lattice [38]. Later, after hopping to the center of the aromatic ring (2) for a few femtoseconds, the Fe atom proceeds to break the C–H bond as demonstrated by the blue hopping path in insert (c). Compared to the C–C bond, the C–H bond in benzene is easier to break, and the C–H breaking in PAHs is regarded as a primary dissociation channel [40,41]. Hence, temperature dependent interactions between metallic Fe and PAH as well as their complex structure should be taken into account in PAH growth and soot nucleation. Movies of the Fe trajectories at 1000 and 1500 K are provided in the Supplemental Material as Movie S1 and S2.

3.2. Fe collisions on PAHs

To further reveal the interplay between the Fe atom and the PAH molecule, dynamic binary collision processes and the resulting structures are scrutinized in this section. Initially, coronene molecules are thermodynamically equilibrated at 500 and 1500 K, and five coronene molecules are sampled from different equilibrium states at each temperature. Three Fe collision energies, namely 0.064, 0.19 and 0.32 eV are selected, which correspond to the mean kinetic energies of a Fe atom at 500, 1500 and 2500 K, respectively. Since binary collision happens in any orientation, a series of collision configurations under the same collision energy are investigated. For each coronene molecule, 1000 independent binary collisions are examined from different collision orientations at the same Fe collision energy to achieve statistical significance as indicated in Fig. 2. Equilibrated coronene molecule locates in the center of a cubic box ($100 \times 100 \times 100$ Å^3), and Fe atoms shown in brown dots are randomly placed in a spherical shell with an initial mass center distance $L_d = 50$ Å from the coronene molecule. The brown arrows represent the collision orientations of Fe atoms towards the coronene molecule including both the center and off-center collisions. Therefore, a total of 30,000 binary collisions are performed during the course of studying PAH fragmentation under Fe collisions.

Fe collisions on the coronene molecules equilibrated at 500 and 1500 K lead to the formation of the following five main structures displayed in Fig. 3. Specifically, Fig. 3(a) shows the coronene molecule remains intact after the Fe collision and the Fe atom reflects back from the surface. Instead of reflecting back, some of the Fe atom is found to stabilize on the coronene surface and locate at the center of outer and inner aromatic rings as shown

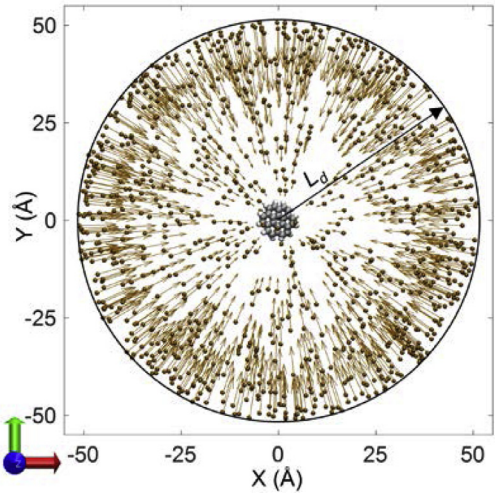

Fig. 2. A summary of the initial configurations of 1000 independent binary collisions of Fe atoms moving towards the coronene molecule at a certain collision energy (viewed from the XY perspective). The coronene molecule is placed in center of a cubic box. Metallic Fe atoms are placed randomly on the spherical surface with a radius of 50 Å centered at (0,0,0). The lengths of the arrows represent the relative values of the collision velocities of Fe atoms towards the coronene molecule.

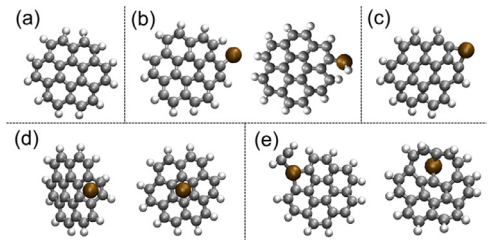

Fig. 3. Different types of structures resulting from Fe collisions. (a) Fe atom flies away by leaving an intact coronene molecule; (b) Fe breaks one C–H bond; (c) Fe breaks two neighboring C–H bonds; (d) Fe stabilizes on the coronene surface; (e) Fe merges with the aromatic rings by breaking the C–C bond.

in Fig. 3(d). On other occasions, PAH fragmentation takes place as Fe collision helps PAH fragmentation through breaking the C–H and/or C–C bonds. Figure 3(b) and (c) demonstrates the structures with one and two neighboring C–H bonds breakup, respectively, accompanied by the Fe atom bonded to the PAH. Finally, Fe is found to merge with the aromatic rings through breaking the C–C bonds as demonstrated in Fig. 3(e) with the Fe atom cooperated to form aromatics containing five or seven membered rings. Movies of the generation of the resulting structures are provided in the Supplemental Material from Movie S3 to S7.

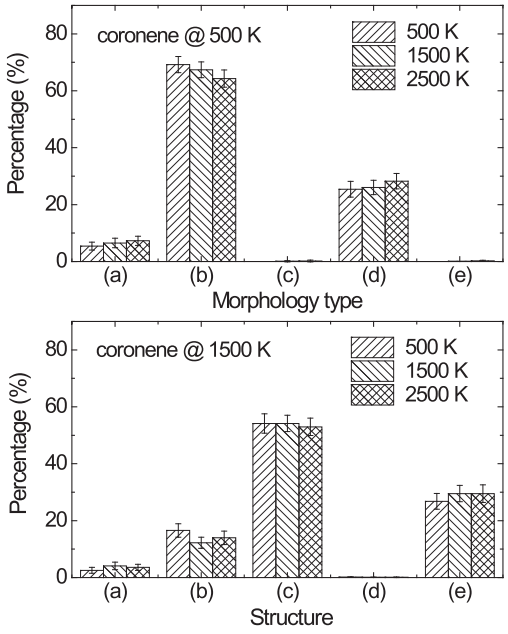

Fig. 4. Percentages of the five main structures (as shown on Fig. 3) formed under Fe collision at collision energy of 0.064, 0.19 and 0.32 eV, which corresponds to Fe kinetic energy at 500, 1500 and 2500 K, respectively. Coronene molecules are equilibrated at 500 K (upper panel) and 1500 K (bottom panel).

Statistical analysis of the percentages of the above five structures produced under different conditions are summarized in Fig. 4, which helps to clarify the underlying correlation among the resulting structure, the Fe collision energy and the PAH equilibrium temperature. Figure 4(a) and (b) is the result of Fe collisions on coronene molecules equilibrated at 500 and 1500 K, respectively. On the whole, changing the collision energy from 0.064 to 0.32 eV, corresponding to the mean kinetic energy of the Fe atom at 500 K to 2500 K, does not seem to significantly influence the percentages of the resulting structures. This is because these collision energies are quite small compared to the strength of the C–H and C–C covalent bonds [22]. The equilibrium temperature of the coronene molecule, however, seems to have a big influence on the resulting structures. For Fe collisions on coronene molecule initially equilibrated at 500 K, structure (b) with one C–H breaking is the most likely outcome (> 60%), followed by structure (d) with Fe resided on the coronene surface (> 20%). However, the possibility of generating structure type (c) with two H abstractions or type (e) of C–C breaking is negligible. The PAH molecule becomes more active when temperature increases to 1500 K, as it is easier to be fragmented through knocking out H and breaking C–C bonds compared to that at 500 K under the same Fe collision energy and orientation. In detail, structure (c) with the breakup of two neighboring C–H bonds is the most frequently observed outcome, followed by structures (e) and (b) in that order. Dynamic processes reveal that structure (c) is developed from structure (b). Therefore, the C–H bond breaking under this condition is still overwhelming. This can be explained by the fact that the C–H fragmentation is the lowest-energy dissociation channel, confirming previous theoretical studies [41–43]. It is noteworthy that structure (d) is not feasible at this temperature, which is consistent with the temperature-dependent structural characteristics of the Fe–PAH complex reported in Section 3.1. The percentage of direct reflection of the Fe atom accounts for less than 10% for the coronene molecule at both temperatures. Results from above demonstrate that the Fe collisions on a PAH molecule at flame temperatures, i.e., 1500 K, is sufficient to assist the PAH fragmentation and generation of PAH radicals which possess higher reactivity than the PAH molecule and probably facilitate later soot nucleation.

In addition, collision orientation of the Fe atom towards the coronene molecule is another important parameter that determines the resulting structures. Here, collisions from Fe atoms at collision energy of 0.19 eV (mean kinetic energy of Fe atom at 1500 K) on the coronene molecule equilibrated at 1500 K are extensively examined. The initial distributions of Fe atoms towards the coronene molecules are displayed on Fig. 5 in terms of the outcomes of resulting structures shown on Fig. 3. Specifically, the Fe atoms that mainly locate in the regions parallel to the coronene surface reflect back after collision, as seen from the front and size views with Fe atoms colored in yellow in Fig. 5(a). On the other hand, Fe atoms leading to structure (b) and (c) are located in most orientations, especially those directed at the side edges of the coronene surface, or more specifically, towards the C–H bonds. Fe atoms that help to break the C–C bond in aromatic rings by forming structure (e) are found to be mostly facing the coronene planar surface according to Fig. 5(e).

3.3. *Fe-assisted PAH nucleation*

After close examination of the structures formed from Fe collisions, we now look into the PAH growth pathway and soot nucleation mechanism in the presence of Fe atoms. In such a system, PAH growth pathway is found to be sensitive to temperature, as demonstrated in Fig. 6 for 1500 and 2500 K. Growth of the PAHs in the presence of Fe atoms is firstly initiated by the dehydrogenation with the Fe atom connecting to the PAH. Then the ($C_{24}H_{11}$–Fe) complex reacts with the colliding coronene molecules by further dehydrogenation and subsequently forming the $(C_{24}H_{11})_2Fe$ complex at 1500 K. This complex is more stable than

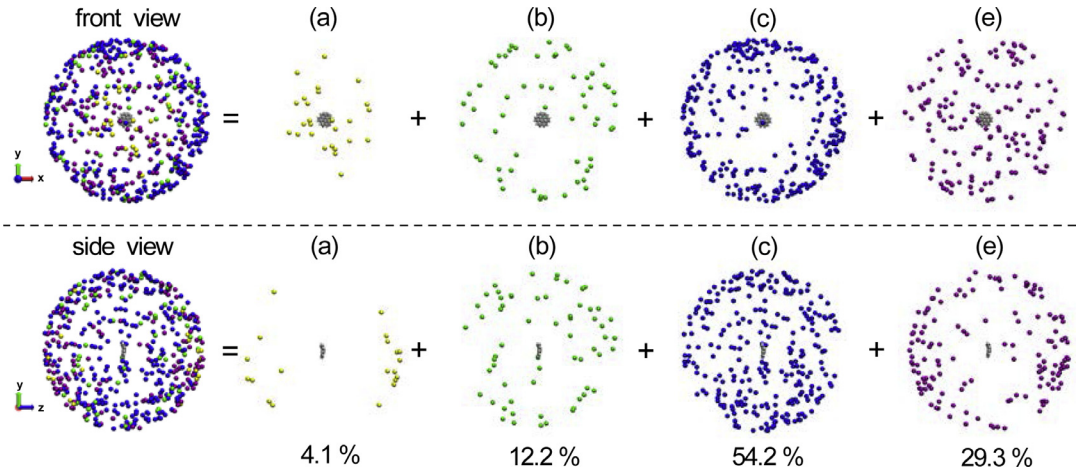

Fig. 5. Distributions of the initial locations of Fe atoms in resulting different structures under collision energy of 0.19 eV on the planar coronene molecule equilibrated at 1500 K. The upper panel and the bottom panel are from the front and size view, respectively. The percentage for the Fe atom in producing each structure is summarized at the bottom.

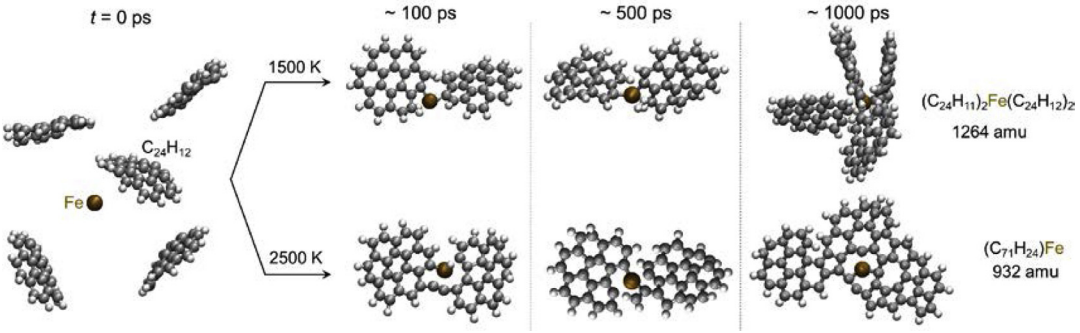

Fig. 6. Key stages of the metallic Fe atom assisted PAH growth pathways at 1500 K (upper panel) and 2500 K (bottom panel).

the coronene dimer formed by dispersive interactions [11,12] as it survives the whole simulation duration after formation. Meanwhile the chemically connected dimer is three-dimensional in configuration similar to the structure proposed in chemical nucleation pathway [2], which further promotes the physical binding with other two intact coronene molecules surrounding by. When the temperature increases to 2500 K, collisions between Fe and coronene molecules facilitate the destruction of the coronene molecule through both C–H and C–C bond breaking, and even ring-opening. Therefore, PAH growth is through recombination of the colliding PAH fragments, and a larger PAH is formed with Fe incorporated to produce embedded five/seven-membered rings.

Finally, quantitative studies of systems containing both coronene monomers and metallic Fe atoms are conducted at temperatures of 1500 K, 2000 K and 2500 K. The results are then compared with systems without Fe addition. Figure 7 reports the mass growth of the maximum clusters (upper panel), together with the number of remaining coronene molecules (bottom panel) at different temperatures. In the pure coronene system ($x_{Fe} = 0$), the largest cluster is just composed of dimers or trimers from 1500 to 2500 K. Meanwhile, the number of coronene molecules does not decrease at 1500 K or 2000 K. This agrees with the previous experimental and theoretical studies of thermal fragmentation of PAHs at about 2200 K [44]. In contrast, the number of coronene molecules decreases dramatically in the system with the Fe mole fraction of 0.167 at all three temperatures, which illustrates the Fe atoms significantly lower the PAH fragmentation temperature by the breakup of C–H and C–C bonds. In addition, the masses of the maximum clusters increase markedly for all above temperatures at the same time. It agrees qualitatively with experimental observation that soot particle size in primary flame zones increases with Fe addition [15,17,18]. As temperature increases to 2000 K

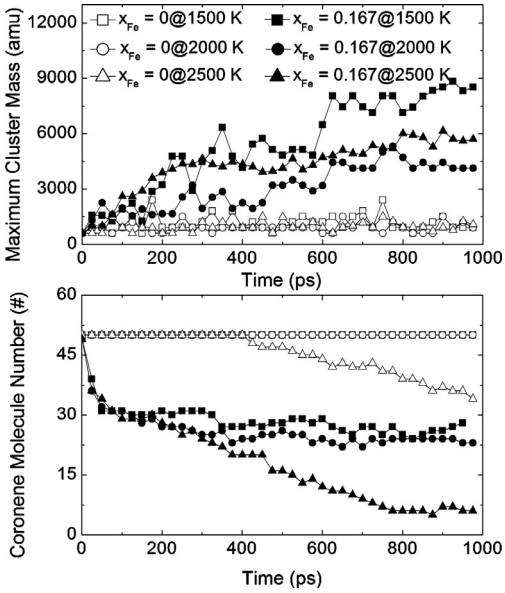

Fig. 7. Mass of the maximum cluster (upper panel) and the number of remaining coronene molecules (bottom panel) formed from the systems composed of pure coronene molecules and systems composed of both coronene molecules and Fe atoms at temperatures from 1500 to 2500 K. Data are sampled at 25 ps intervals.

and 2500 K, the mass of the largest clusters formed in the presence of Fe atoms is lighter compared to that at 1500 K. This phenomenon can be explained by the combined physical and chemical nucleation at 1500 K and the pure chemical mechanism at 2500 K, as illustrated in Fig. 6. At 2000 K, the decrease in the number of coronene molecules is similar to that at 1500 K but the possibility of physical growth decreases compared to that at 1500 K, hence resulting in the lowest soot mass.

4. Conclusions

In this paper, impact of Fe atoms on the PAH fragmentation, growth and soot nucleation is revealed through performing ReaxFF-based reactive MD simulations. The diffusivity of Fe atoms on the PAH surface is found to be highly dependent on temperature. That is, the Fe atoms on PAH surfaces preferentially stabilize around their binding sites at low temperatures, while they hop frequently between sites and some even merging with the PAH molecule by breaking the C–H bond at elevated temperatures. Five typical types of structures have been observed as a result of Fe collision at different collision energies and orientations. It is found that the resulting structures are sensitive to the initial equilibrium temperature of PAH molecules. Under the same Fe collision energy, structures with one C–H bond breaking and a Fe atom stabilized on the aromatic rings are commonly observed for PAHs initially equilibrated at 500 K. In contrast, structures with two H abstractions and C–C bond breaking are the most predominant when increasing the PAH equilibrium temperature to 1500 K. In addition, PAH growth and soot nucleation are enhanced dramatically in the presence of Fe atoms, leading to faster growth and larger clusters compared to the pure PAH system at typical flame temperatures (1500–2500 K). This is due to the fact that the Fe atoms significantly lower the PAH fragmentation temperature. The pathways for PAH growth and soot nucleation, however, are also highly dependent on temperature. At 1500 K, soot nucleation results from both physical and chemical mechanisms as Fe firstly helps the dehydrogenation and connects PAHs by strong covalent bonds. The newly formed larger PAHs further facilitate physical binding with other intact PAH molecules. Nevertheless, a pure chemical mechanism is at work at higher temperatures (e.g., 2500 K) as the Fe atoms merge with aromatic rings to form embedded five/seven-membered rings during the PAH growth. The atomic level understanding obtained from the ReaxFF-MD simulations of this study provides further insight into the complex mechanism of PAH growth and soot nucleation in the presence of trace metal atoms in a more realistic combustion system.

Acknowledgments

Support from the National Natural Science Foundation of China (Grant Nos. 91441120 and 51390493) is gratefully acknowledged. The simulations were partly performed on the Tsinghua High-Performance Parallel Computer supported by the Tsinghua National Laboratory for Information Science and Technology and partly on ARCHER funded under the EPSRC projects "UK Consortium on Mesoscale Engineering Sciences (UKCOMES)" (Grants No. EP/L00030X/1 and No. EP/R029598/1) and "High Performance Computing Support for United Kingdom Consortium on Turbulent Reacting Flow (UKCTRF)" (Grant No. EP/K024876/1).

Supplementary materials

Supplementary material associated with this article can be found, in the online version, at doi:10.1016/j.proci.2018.06.106.

References

[1] H. Bockhorn, A. D'Anna, A.F. Sarofim, H. Wang, *Combustion Generated Fine Carbonaceous Particles*,

Karlsruhe University Press, Villa Orlandi, Anacapri, 2007.
[2] H. Wang, *Proc. Combust. Inst.* 33 (2011) 41–67.
[3] K.O. Johansson, T. Dillstrom, P. Elvati, et al., *Proc. Combust. Inst.* 36 (2017) 799–806.
[4] M.E. Mueller, G. Blanquart, H. Pitsch, *Proc. Combust. Inst.* 33 (2011) 667–674.
[5] H.A. Michelsen, *Proc. Combust. Inst.* 36 (2017) 717–735.
[6] Q. Tang, R. Cai, X. You, J. Jiang, *Proc. Combust. Inst.* 36 (2017) 993–1000.
[7] H. Sabbah, L. Biennier, S.J. Klippenstein, I.R. Sims, B.R. Rowe, *J. Phys. Chem. Lett.* 1 (2010) 2962–2967.
[8] J.D. Herdman, J.H. Miller, *J. Phys. Chem. A* 112 (2008) 6249–6256.
[9] T.S. Totton, D. Chakrabarti, A.J. Misquitta, M. Sander, D.J. Wales, M. Kraft, *Combust. Flame* 157 (2010) 909–914.
[10] S.H. Chung, A. Violi, *Proc. Combust. Inst.* 33 (2011) 693–700.
[11] Q. Mao, A.C.T. van Duin, K.H. Luo, *Carbon* 121 (2017) 380–388.
[12] Q. Mao, Y. Ren, K.H. Luo, A.C.T. van Duin, *J. Chem. Phys.* 147 (2017) 244305.
[13] T.S. Totton, A.J. Misquitta, M. Kraft, *Phys. Chem. Chem. Phys.* 14 (2012) 4081–4094.
[14] J.B. Howard, W.J. Kausch, *Prog. Energy Combust. Sci.* 6 (1980) 263–276.
[15] K.E. Ritrievi, J.P. Longwell, A.F. Sarofim, *Combust. Flame* 70 (1987) 17–31.
[16] A.S. Feitelberg, J.P. Longwell, A.F. Sarofim, *Combust. Flame* 92 (1993) 241–253.
[17] J. Zhang, C.M. Megaridis, *Combust. Flame* 105 (1996) 528–540.
[18] T. Hirasawa, C.J. Sung, Z. Yang, A. Joshi, H. Wang, *Combust. Flame* 139 (2004) 288–299.
[19] P. Glarborg, *Proc. Combust. Inst.* 31 (2007) 77–98.
[20] K.B. Kim, K.A. Masiello, D.W. Hahn, *Combust. Flame* 154 (2008) 164–180.
[21] M.P. Herring, P.M. Potter, H. Wu, S. Lomnicki, B. Dellinger, *Proc. Combust. Inst.* 34 (2013) 1749–1757.
[22] S. Kolakkandy, S. Pratihar, A.J.A. Aquino, H. Wang, W.L. Hase, *J. Phys. Chem. A* 118 (2014) 9500–9511.
[23] J. Reader, J. Sugar, *J. Phys. Chem. Ref. Data* 4 (1975) 353–440.
[24] M.N. Saha, *Philos. Mag. J. Sci.* 40 (1920) 472–488.
[25] Y. Ren, W. Cui, S. Li, *Phys. Rev. E* 97 (2018) 1–8.
[26] S. Plimpton, *J. Comput. Phys.* 117 (1995) 1–19.
[27] W. Humphrey, A. Dalke, K. Schulten, *J. Mol. Graph.* 14 (1996) 33–38.
[28] A. Stukowski, *Model. Simul. Mater. Sci. Eng.* 18 (2010) 015012.
[29] K. Chenoweth, A.C.T. van Duin, W.A. Goddard, *J. Phys. Chem. A* 112 (2008) 1040–1053.
[30] T. Senftle, S. Hong, M.M. Islam, et al., *The Npj Comput. Mater.* 2 (2016) 15011.
[31] S. Goverapet Srinivasan, A.C.T. van Duin, P. Ganesh, *J. Phys. Chem. A* 119 (2015) 571–580.
[32] M.M. Islam, C. Zou, A.C.T. van Duin, S. Raman, *Phys. Chem. Chem. Phys.* 18 (2016) 761–771.
[33] J.P. Perdew, K. Burke, M. Ernzerhof, *Phys. Rev. Lett.* 77 (1996) 3865–3868.
[34] A.D. Becke, *J. Chem. Phys.* 98 (1993) 5648–5652.
[35] C. Lee, W. Yang, R.G. Parr, *Phys. Rev. B* 37 (1988) 785–789.
[36] S. Grimme, *J. Comput. Chem.* 27 (2006) 1787–1799.
[37] X. Sun, Y. Yamauchi, M. Kurahashi, T. Suzuki, Z.P. Wang, S. Entani, *J. Phys. Chem. C* 111 (2007) 15289–15298.
[38] A.W. Robertson, B. Montanari, K. He, et al., *Nano Lett.* 13 (2013) 1468–1475.
[39] D. Frenkel, B. Smit, *Understanding Molecular Simulation: from Algorithms to Applications*, Academic Press, 1996.
[40] G.E. Davico, V.M. Bierbaum, C.H. DePuy, G.B. Ellison, R.R. Squires, *J. Am. Chem. Soc.* 117 (1995) 2590–2599.
[41] B. West, F. Useli-Bacchitta, H. Sabbah, et al., *J. Phys. Chem. A* 118 (2014) 7824–7831.
[42] S. Martin, L. Chen, R. Brédy, et al., *Phys. Rev. A* 85 (2012) 1–8.
[43] R. Delaunay, M. Gatchell, P. Rousseau, et al., *J. Phys. Chem. Lett.* 6 (2015) 1536–1542.
[44] T. Chen, M. Gatchell, M.H. Stockett, et al., *J. Chem. Phys.* 142 (2015) 144305.